Applied Catalysis B: Environmental 154–155 (2014) 16–26

Contents lists available at ScienceDirect

Applied Catalysis B: Environmental

journal homepage: www.elsevier.com/locate/apcatb

Kinetic modelling of Pt and Pt:Pd diesel oxidation catalysts

M. Khosravi[a], A. Abedi[b], R.E. Hayes[a,*], W.S. Epling[b,c], M. Votsmeier[d]

[a] Department of Chemical and Materials Engineering, University of Alberta, Edmonton, AB, Canada
[b] Department of Chemical Engineering, University of Waterloo, Waterloo, ON, Canada
[c] Departments of Chemical and Bimolecular Engineering, University of Houston, Houston, TX, USA
[d] Umicore, Automotive Catalysis Division, Research and Development, Hanau, Germany

ARTICLE INFO

Article history:
Received 11 October 2013
Received in revised form 27 January 2014
Accepted 1 February 2014
Available online 12 February 2014

Keywords:
Nitrous oxide
Propene
Oxidation
Reduction

ABSTRACT

This paper describes an experimental and theoretical investigation of the oxidation of carbon monoxide, nitrogen monoxide and propene, and the reduction of nitrogen monoxide by propene over two diesel oxidation catalysts. Synthetic exhaust gas mixtures are used. The catalysts were commercial monolith samples of 400 CPSI with a total PGM loading of 95 g/ft^3. One monolith had platinum catalyst only, and the other was a bimetallic catalyst of 4:1 by mass platinum and palladium. The bimetallic catalyst was more active, and showed a different behaviour for propene oxidation than the Pt only catalyst. Global kinetic models for the oxidation of CO, C_3H_6, and NO, and the selective catalytic reduction of NO to N_2 and N_2O are developed. A good agreement between experimental results and simulation is observed.

1. Introduction

The control of automotive emissions from automotive sources is a challenging reaction engineering application. The emissions of interest are carbon monoxide (CO), hydrocarbons (HC) and oxides of nitrogen (NO and NO_2). The treatment of exhaust gas emissions is primarily achieved using one or more catalytic converters. Typically, these converters consist of a honeycomb substrate (ceramic or metal), the channels of which are coated with a washcoat containing a catalyst. For spark ignition (SI) engines with stoichiometric operating condition, the three way catalytic converter (TWC) is used to oxidize carbon monoxide and hydrocarbon residuals and reduce NO_X content, using two different catalysts. This technology cannot be used in lean burn engines, such as compression ignition Diesel engines, because of the presence of excess oxygen. To conquer this problem, a combination of two types of converters in series is typically employed. The first converter is the diesel oxidation catalyst (DOC) which oxidizes CO and HC to CO_2 and H_2O. Some NO is oxidized to NO_2, and some N_2O and N_2 can also be formed. This converter usually uses platinum or platinum and palladium mixtures as the active catalyst. The second catalytic converter is used to remove NO and NO_2 from the exhaust, and usually uses selective catalytic reduction [1]. A NO_X trap catalyst may also be used.

Computer modelling can be used to aid the design of catalytic converter systems, and such simulations require good kinetic models for the catalyst in question. Although there have been many publications in recent years detailing the use of mechanistic kinetic models, by and large the use of more empirical global models is most commonly practiced. For catalytic converter applications, the work of Voltz et al. [2] is a common starting point. Their models are essentially of the LHHW type, and although the original work was limited to CO and HC oxidation, in the presence of non-reacting NO, the models have since been extended to a variety of more complex situations [3–12].

The objective of this research was to determine global kinetic models for Pt and Pt:Pd diesel oxidation catalysts. This work is the third paper in a sequence that includes the work of Sola et al. [6], who studied CO and C_3H_6 oxidation over Pt catalyst, and of Khosravi et al. [13], who studied selective catalytic reduction (SCR) of NO by C_3H_6 over Pt and Pt:Pd catalysts.

2. Experimental

2.1. Methodology

The experimental procedures used were essentially the same as described earlier [6,13] however, for completeness are briefly repeated here. Experimental data were obtained on a Pt and a Pt:Pd diesel oxidation catalyst (DOC) in the form of a washcoated ceramic monolith with 400 cells per square inch (CPSI). The catalyst was supplied by Umicore, AG. The total precious metal loading was

* Corresponding author. Tel.: +1 780 492 3571; fax: +1 780 492 2881.
E-mail address: bob.hayes@ualberta.ca (R.E. Hayes).

http://dx.doi.org/10.1016/j.apcatb.2014.02.001
0926-3373/

Table 1
CO, H_2, Propene and NO experiments, initial concentrations used for the Pt catalyst. Concentrations in ppm by volume.

Run	CO	H_2	Propene	NO
23a	500	167	500	150
24a	750	250	500	150
26a	1250	417	500	150
27a	1500	500	500	150
28a	2000	666	500	150
29a	500	167	250	300
30a	750	250	750	300
31a	1000	333	750	600
32a	1500	417	750	600
33a	2000	666	750	600

Table 2
CO, H_2, Propene and NO experiments, initial concentrations used for the Pt:Pd catalyst. Concentrations in ppm by volume.

Run	CO	H_2	Propene	NO
28b	500	167	250	150
29b	2000	666	250	150
30b	500	167	750	150
31b	2000	666	750	150
32b	500	167	250	600
33b	2000	666	250	600
34b	500	167	750	600
35b	2000	666	750	600
36b	1000	333	250	150
37b	1000	333	250	600
38b	1000	333	750	150
39b	1000	333	750	600
40b	500	167	500	150
41b	2000	666	500	150
42b	500	167	500	600
43b	2000	666	500	600
44b	500	167	250	300
45b	2000	666	250	300
46b	500	167	750	300
47b	2000	666	750	300
48b	1000	333	500	150
49b	1000	333	250	300
50b	500	167	500	300
51b	1000	333	500	300
52b	2000	666	500	300
53b	1000	333	750	300
54b	1000	333	500	600

95 g/ft^3 based on total monolith volume for both catalysts. For the bimetallic catalyst, the Pt loading was four times the Pd loading on a mass basis. Cylindrical monolith cores were cut from a full size converter. The cores were 2.29 cm in diameter and 6.10 cm long, giving a reactor volume of 25 cm^3. The cores were wrapped in 3 M insulation material and inserted into a horizontal quartz tube. The tube was placed inside of a Lindberg Minimite temperature controlled furnace. K-type thermocouples inserted into the monolith channels gave the temperatures at four axial locations, 0 cm, 2 cm, 4 cm and 6 cm from the monolith inlet. The catalyst was aged at 650 °C in flowing air for 16 h prior to use.

Each experiment consisted of an ignition curve. We mention that hysteresis was observed in the experiments when ignition and extinction curves were performed. Reaction rate parameters will thus be influenced by reversible deactivation effects, and this point should be noted when considering parameter values in the proposed rate functions. The initial feed stream temperature was fed to the reactor below 80 °C, to avoid reaction before ramping. The temperature was then ramped at 3 °C/min. When complete oxidation was achieved, the reactor was cooled by decreasing the furnace temperature to below 80 °C. The base feed stream consisted of 10% O_2, 10% H_2O, 10% CO_2, 300 ppm or 1% He, appropriate reactant gases, with N_2 as the balance. He was included to aid in analysis using an inline mass spectrometer. The mass spec was not used in these tests, but He was included in the feed at all times. The total gas flow rate was 9.34 L/min referenced to 298 K and 1 atm pressure. The corresponding space velocity is 20,520 h^{-1} at STP (273 K and 1 atm). The outlet gas composition was measured using a MultiGas 2030 FTIR analyzer (MKS). Before running any experiment, a test with N_2 only (no reactant) was performed to check the temperature difference between the front and the back of the catalyst as well as the radial direction. The test showed that the maximum difference was less than 5 ◦C between the front and the back and 4 °C in the radial direction (which occurred at high temperature).

The reactants in the feed consisted of CO, H_2, C_3H_6 and NO. The inlet concentrations of the reactants used in the experiments are given in Table 1 for the Pt catalyst and Table 2 for the Pt:Pd catalyst. The concentrations are given in ppm on a volumetric (molar) basis. Note that in all experiments, the hydrogen concentration was one third of the CO concentration.

Temperature and outlet concentration data were measured every second. This very large data set was reduced in size for the reactor modelling exercise to decrease computational cost. Data points were extracted from the large data set for every change in conversion of the order of 5% or a temperature change of 5 °C, whichever was smaller.

2.2. Results

Prior to the discussion of modelling, we present in this section some typical experimental results for each catalyst, as they show some critical features of the ignition curves. Fig. 1(a) shows the ignition curves obtained for the platinum only catalyst, run number 23a, and (b) for the Pt:Pd catalyst, run 42b. The general appearance of the curves is similar to that reported elsewhere, and is consistent with [13]. The oxidation of CO occurs first, followed by that of C_3H_6. As the propene begins to oxidize, it reacts with NO to produce N_2 and N_2O, and finally NO is oxidized to NO_2 as the C_3H_6 vanishes. There are no significant surprises for the Pt catalyst in terms of general effects, however, for the Pt:Pd catalyst there is a different shape for the propene ignition curve. It is divided into two distinct regions, with a noticeable change in slope, and in some cases a plateau, in the conversions between them. This behaviour was not seen for the same conditions in the absence of CO [13]. In Fig. 2, for example, we have superimposed the equivalent ignition curves for the same experiment done without CO for the Pt:Pd catalyst (run 18 from Ref. [13]). The lines represent the behaviour without CO, and the symbols the conversions with CO present. The difference in shape of the propene ignition curve is evident. From an examination of all of the results, it was apparent that the slope change tended to happen at the point where the outlet CO conversion was close to 100%.

The shape of the propene ignition curve was also observed to depend on the feed concentration. For example, experiments 34b and 35b are compared in Fig. 3. Both experiments used 750 ppm C_3H_6 and 600 ppm NO, but the CO concentrations were 500 and 2000 ppm for experiments 34b and 35b, respectively. The symbols in Fig. 3 represent experiment 34b, and the lines experiment 35b. It is seen that the conversion of NO is essentially the same, including the product distribution, while the ignition curve of CO has moved to the right (dashed line in Fig. 3) as expected, owing to its self-inhibition. The change in shape of the C_3H_6 ignition curve is seen, and we note that the change in slope coincides with the point of compete CO conversion at the reactor outlet.

The shape of the propene oxidation curve was also affected by the NO concentration. Fig. 4 shows the propene oxidation curves for experiments 28b and 32b. Both these runs used 500 ppm CO and 250 ppm C_3H_6, but with NO concentrations of 150 (exp 28b)

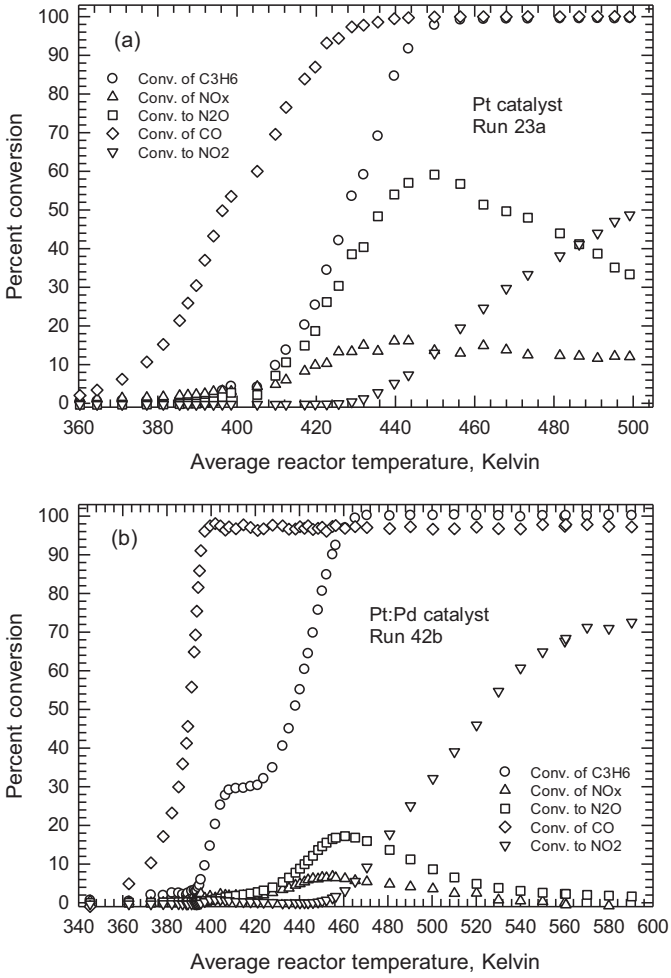

Fig. 1. Typical ignition curves observed for the complete exhaust gas mixture over two catalysts. (a) Mono-metallic Pt catalyst, corresponding to run 23a and (b) bi-metallic Pt:Pd catalyst corresponding to Run 42b.

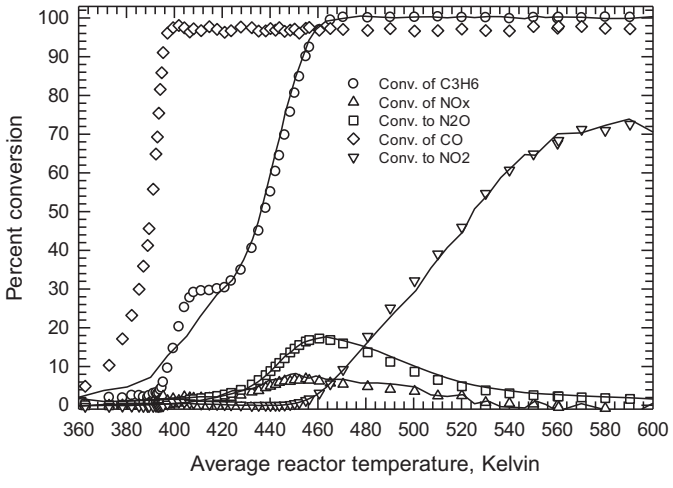

Fig. 2. Ignition curves for the Pt:Pd catalyst in the presence and absence of CO. The symbols represent the results from experiment 42b, while the solid lines are the ignition curves obtained for the same conditions but without CO in the feed. The effect of CO on the ignition of propene is evident.

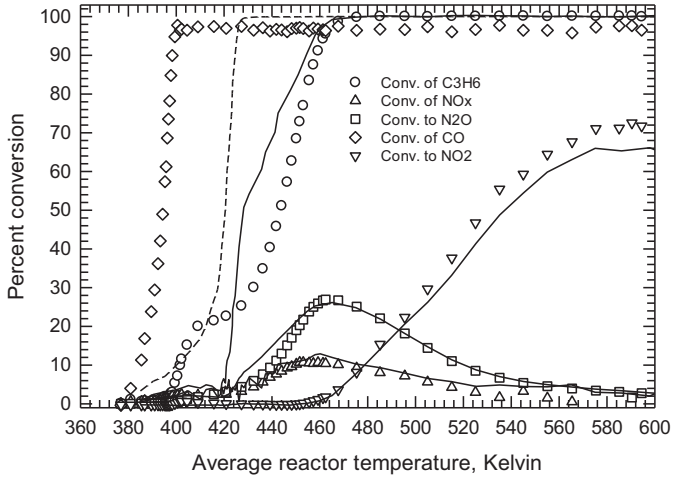

Fig. 3. Comparison of experiments 34b and 35b. Both experiments used 750 ppm C_3H_6 and 600 ppm NO, but the CO concentrations were 500 and 2000 ppm for experiments 34b and 35b, respectively. The symbols represent experiment 34b, and the lines experiment 35b. The dashed line is the CO conversion for experiment 35b.

and 600 (exp 32b) ppm, respectively. The higher NO concentration causes a sharper deviation with concomitant flat area. The symbols represent experiment 28b and the lines experiment 32b. Note also that the increase in NO concentration suppresses the catalytic reduction of NO, and the conversion to NO_2 is essentially the same. Clearly, the propene ignition curve provides a modelling challenge, and to the best of our knowledge this behaviour has not been reported before, let alone modelled.

3. Modelling

3.1. Reactor model

To determine the best fit for the kinetic parameters, a reactor model is necessary. The model used was the same as described by Khosravi et al. [13], and is briefly summarized here. To achieve a low CPU time, a one dimensional pseudo-homogeneous steady state plug flow single channel model (SCM) was used. Only the appropriate mass conservation equations are solved, and not the energy balance. The reactor temperature measured at each time step was

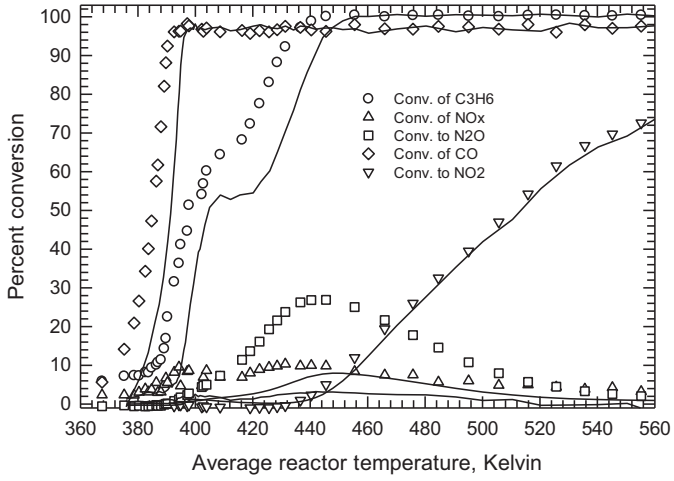

Fig. 4. Comparison of experiments 28b and 32b. Both these runs used 500 ppm CO and 250 ppm C_3H_6, but with NO concentrations of 150 (exp 28b) and 600 (exp 32b) ppm, respectively. The higher NO concentration causes a sharper deviation with concomitant flat area. The symbols represent experiment 28b and the lines experiment 32b.

imposed in the model, with linear interpolation used for the points between the measured values. Because the temperature along the centre line of the reactor is known at four locations, the simulator uses these four temperatures to impose a temperature profile along the reactor. Linear interpolation was used between the measured points.

Even though the experiments are transient, it is acceptable to use a steady state model. The residence time in the reactor is very small, of the order of 0.02 s. The temperature change of the solid is much slower, so in effect the gas is always in a pseudo-steady state with the wall temperature. Because the temperature is measured, the steady state model will give a good solution. The ignition curve was constructed by performing a sequence of steady state simulations with increasing reactor temperatures, based on the experimental values.

The mole balance equation is written for each species of interest. For species j we have:

$$-Cu_m \frac{dY_j}{dz} - \left(-R_j\right)\frac{V_W}{V_C} = 0 \tag{1}$$

The mean velocity in the channel is denoted u_m and the bulk molar concentration of the gas is C, which is computed from the ideal gas law. The product of velocity and bulk molar concentration is a constant. The reaction rate was based on the washcoat volume. It was converted to a basis of channel volume for the homogeneous reactor model using the ratio of washcoat volume (V_W) and the channel volume (V_C). If the channel is approximated as a right circular cylinder of a length of z, diameter D_H, with the washcoat occupying an annular ring of outside diameter D_{WC}, then with the appropriate substitution, we obtain

$$-Cu_m \frac{dY_j}{dz} - \left(-R_j\right)_V \frac{\left({D_{WC}}^2 - {D_H}^2\right)}{{D_H}^2} = 0 \tag{2}$$

This equation can be explicitly arranged to give

$$-\frac{dY_j}{dz} = \frac{\left(-R_j\right)_V}{Cu_m}\frac{\left({D_{WC}}^2 - {D_H}^2\right)}{{D_H}^2} \tag{3}$$

The resulting kinetic parameters are therefore global, in that they include all heat and mass transfer effects implicitly, and are not intrinsic rate constants. Substitution of all constants into the mole balance equation gives

$$-\frac{dY_j}{dz} = 7.688 \times 10^{-3}\left(-R_j\right)_V \tag{4}$$

The software MATLAB was used to solve the differential equations simultaneously. The NAG toolbox solver, "d02ej" was used, which was almost two times faster than regular MATLAB solvers (e.g. ode15s or ode45).

3.2. Parameter estimation

The optimization method described in Ref. [13] used the MATLAB algorithm fmincon as the main optimization tool. This gradient based algorithm attempts to find a constrained minimum of a scalar multivariable function starting at an initial point. To avoid being trapped in a local minimum, a good initial guess is essential. To obtain a good initial guess, a genetic algorithm (GA) was used as a preliminary optimizer. Combining these two methods gave excellent results.

The objective function was defined in terms of the fractional conversion of a reactant into a designated product. The general formula for species j can be written:

$$O_j = \frac{1}{2}\sum_{i=1}^{n}\left(X_{\mathrm{exp},i} - X_{\mathrm{pred},i}\right)^2 \tag{5}$$

The kinetic models used here contain kinetic and adsorption parameters in the Arrhenius form. As an aid in optimization, these parameters were written in the following form:

$$k_i = \exp\left(A_i - \frac{E_i}{R_g}\left[\frac{1}{T} - \frac{1}{450}\right]\right) \tag{6}$$

$$K_i = \exp\left(B_i - \frac{H_i}{R_g}\left[\frac{1}{T} - \frac{1}{450}\right]\right) \tag{7}$$

The temperature of 450 K was used in the exponential, being in the central region of the ignition curves for the experimental range of conditions considered. Expressing the rate parameters in this form gave a much more stable and efficient algorithm.

For clarity, we state here explicitly the basis for calculating the fractional conversions for the NO_X compounds. Because the NO that reacts produces NO_2, N_2 and N_2O, we have to define fractional conversions on this basis, as follows:

(a) The conversion of NO to NO_2 as:

$$X_{NO_2} = \frac{\left(Y_{NO_2}\right)_f}{(Y_{NO})_0} \tag{8}$$

(b) The conversion of NO to N_2O as:

$$X_{N_2O} = \frac{2\left(Y_{N_2O}\right)_f}{(Y_{NO})_0} \tag{9}$$

(c) The conversion of NO to N_2 (that is, NO_X conversion) as:

$$X_{NO_X} = \frac{(Y_{NO})_0 - \left[(Y_{NO})_f + 2\left(Y_{N_2O}\right)_f + \left(Y_{NO_2}\right)_f\right]}{(Y_{NO})_0} \tag{10}$$

3.3. Kinetic model for the platinum catalyst

It is seen in Section 2.2 that the Pt:Pd catalyst showed a significantly different shape for the propene ignition curve than was seen with the Pt catalyst. We therefore discuss the models proposed for each catalyst in turn, starting with the Pt catalyst.

The kinetic model must account for each of the reactions. The oxidation reactions written in global form are

$$CO + \frac{1}{2}O_2 \rightarrow CO_2 \tag{11}$$

$$C_3H_6 + \frac{9}{2}O_2 \rightarrow 3CO_2 + 3H_2O \tag{12}$$

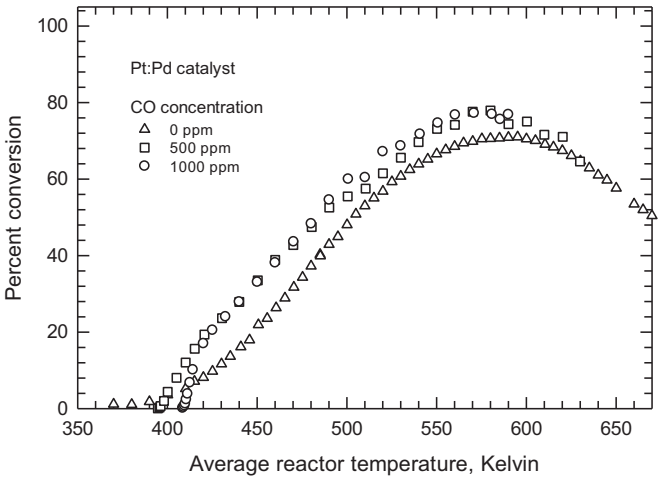

Fig. 5. Effect of CO concentration on the oxidation of NO for the Pt:Pd catalyst. The NO concentration was 600 ppm.

$$H_2 + \frac{1}{2}O_2 \rightarrow H_2O \quad (13)$$

$$NO + \frac{1}{2}O_2 \rightleftharpoons NO_2 \quad (14)$$

Over a PGM catalyst, SCR can be represented by the following global reactions:

$$C_3H_6 + 2NO + \frac{7}{2}O_2 \rightarrow N_2 + 3H_2O + 3CO_2 \quad (15)$$

$$C_3H_6 + 2NO + 4O_2 \rightarrow N_2O + 3H_2O + 3CO_2 \quad (16)$$

We can also potentially have the reaction between NO_2 and propene to form NO:

$$C_3H_6 + NO_2 + 4O_2 \rightarrow NO + 3H_2O + 3CO_2 \quad (17)$$

As a starting point in the construction of a kinetic model, we use as a foundation the work of Sola et al. [6] and Khosravi et al. [13]. The reader should especially refer to Ref. [13] for the model discrimination work on the NO oxidation and SCR reactions. It is known that there are many interactions among the reactants for the feed used in these experiments. For example, hydrogen is known to enhance the oxidation of CO by lowering the activation energy for CO desorption [10,14]. Although the effect can be modelled in a mechanistic scheme [14], the practice in the literature is to use the

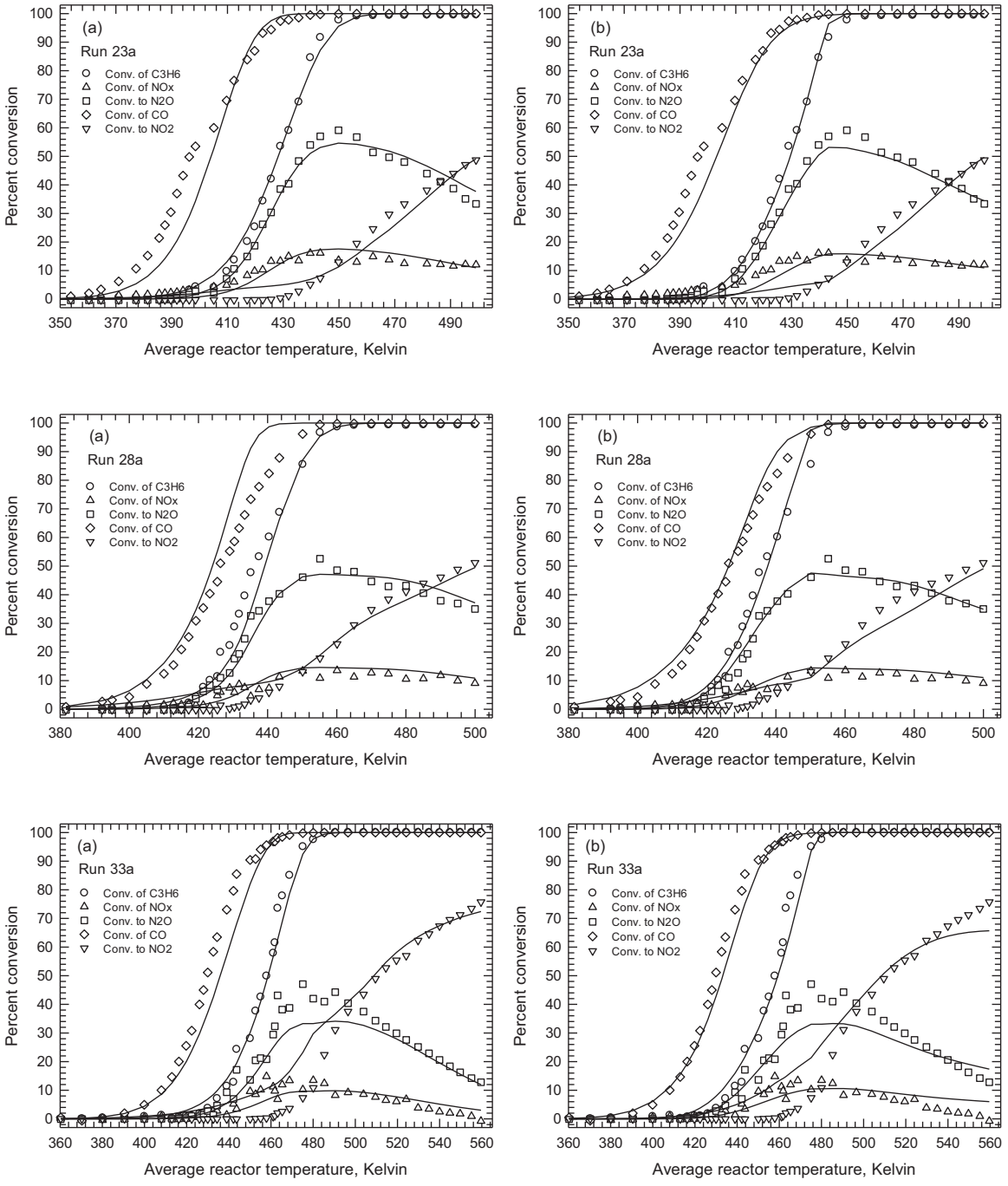

Fig. 6. Comparison of the experimental and model results for three experiments for the platinum catalyst. The symbols are the experimental points and the lines are the model predictions. (a) Model A and (b) Model B. The simulated results are calculated using the parameters optimized using experiments 23a, 28a, 29a, 31a and 33a.

same model for hydrogen oxidation as is used for CO oxidation [12], replacing the CO concentration in the model by the H_2 concentration and keeping the same model parameters [12]. This approach is reasonable, because the hydrogen oxidizes very shortly after the CO does. CO and C_3H_6 both exhibit self-inhibition, and also inhibit the oxidation of each other [2,6]. NO and C_3H_6 also show mutual inhibition [13]. The interactions of NO with propene are thoroughly discussed in Ref. [13], and the remaining issue is the effect of CO on the NO oxidation. From Fig. 2 we can see that there is no apparent effect on NO of the addition of CO to the mixture. If we consider the case when there is only CO and NO in the feed, it appears that there is a small enhancement of NO oxidation by the presence of CO. This effect is shown in Fig. 5 for the Pt:Pd catalyst. However, when the entire mixture is used, because the presence of CO dominates, followed by hydrocarbon, it is not surprising that the oxidation of NO is not significantly affected by CO when propene is present. We also recall from Ref. [13] that the effect of propene is to delay the onset of NO oxidation. This delay can be quantified by the addition of an inhibition term for C_3H_6 in the NO oxidation rate equation, however, when only mixtures are to be modelled, such a term is not necessary [13]. Therefore did not include inhibition terms for CO or C_3H_6 in the NO oxidation rate equation.

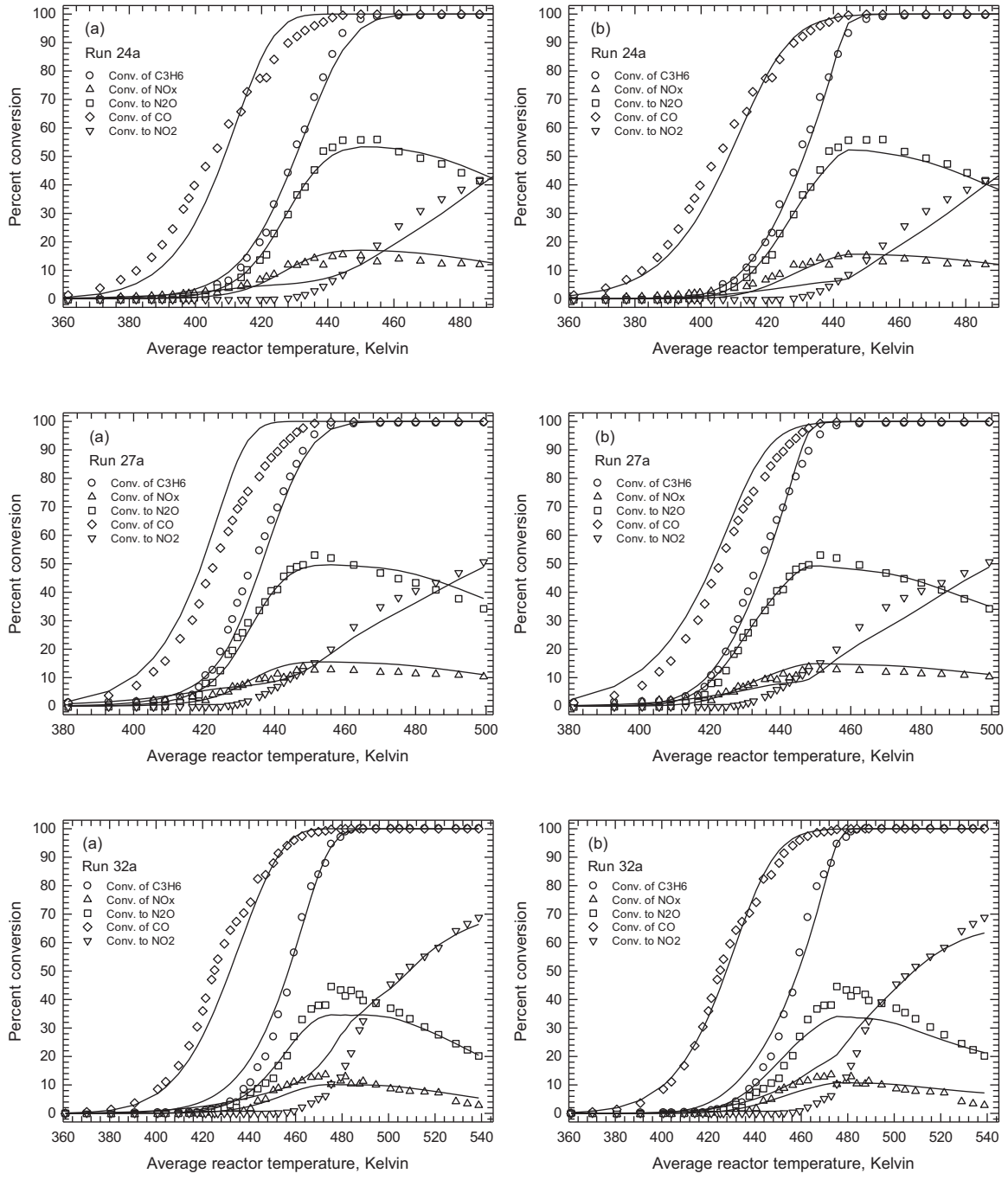

Fig. 7. Comparison of the experimental and model results for three experiments for the platinum catalyst. The symbols are the experimental points and the lines are the model predictions. (a) Model A and (b) Model B. The simulated results are calculated using the parameters optimized using experiments 24a, 26a, 27a, 30a and 32a, which includes the experiments shown here.

Table 3
Residuals for Models A and B for the platinum catalyst experiments.

Exp.	model	CO	HC	NO_X	N_2O	NO_2	Total
23a	A	55.7	3.4	4.5	4.0	7.9	75.4
23a	B	27.7	3.6	6.0	3.8	5.3	46.4
24a	A	39.7	5.2	2.8	3.1	11.0	61.8
24a	B	16.0	3.6	2.8	2.4	7.9	32.7
26a	A	81.6	8.7	6.2	4.3	15.4	116.3
26a	B	30.9	7.7	4.4	2.7	13.7	59.4
27a	A	95.3	16.3	4.2	5.2	17.0	138.0
27a	B	28.2	12.9	3.3	2.6	15.2	62.3
28a	A	75.8	21.5	4.1	7.5	19.5	128.4
28a	B	9.9	11.7	4.0	5.7	15.8	47.1
29a	A	43.7	34.8	2.1	10.1	137.9	228.7
29a	B	27.4	3.1	2.5	9.5	83.9	126.4
30a	A	167.1	30.2	0.7	12.5	12.2	222.6
30a	B	84.9	6.4	1.3	4.0	8.4	105.1
31a	A	53.3	99.3	3.4	22.7	55.3	234.0
31a	B	12.3	69.5	2.7	27.9	50.2	162.6
32a	A	36.0	16.0	2.7	11.9	39.8	106.4
32a	B	7.0	17.8	3.1	14.0	38.5	80.3
33a	A	44.5	9.3	6.3	24.8	45.8	130.8
33a	B	13.9	8.9	8.7	21.2	51.8	104.4

Based on these observations, we started with the most successful model for the SCR presented by Khosravi et al. [13], and add in the necessary terms to account for the presence of CO. We review now some of the key observations from Refs. [6,13]. The original Voltz model can be represented as:

$$(-R_{CO}) = \frac{k_1 Y_{CO} Y_{O_2}}{R_I} \tag{18}$$

and:

$$\left(-R_{C_3H_6}\right) = \frac{k_3 Y_{C_3H_6} Y_{O_2}}{R_I} \tag{19}$$

In these equations R_I is the adsorption inhibition term, given by:

$$R_I = \left(1 + K_5 Y_{CO} + K_6 Y_{C_3H_6}\right)^2 \left(1 + K_7 \left(Y_{CO} Y_{C_3H_6}\right)^2\right) \left(1 + K_8 (Y_{NO})^{0.7}\right) \tag{20}$$

The denominator was subsequently modified by the addition of a temperature by [3]:

$$R_I = T\left(1 + K_5 Y_{CO} + K_6 Y_{C_3H_6}\right)^2 \left(1 + K_7 \left(Y_{CO} Y_{C_3H_6}\right)^2\right) \left(1 + K_8 (Y_{NO})^{0.7}\right) \tag{21}$$

A slightly different dependency for NO was used by [8]

$$R_I = T\left(1 + K_5 Y_{CO} + K_6 Y_{C_3H_6}\right)^2 \left(1 + K_7 \left(Y_{CO} Y_{C_3H_6}\right)^2\right) (1 + K_8 Y_{NO}) \tag{22}$$

In Ref. [6], in a study limited to CO and C_3H_6 over the Pt catalyst, it was observed that the term for the cross dependency of CO and C_3H_6 (K_7) did not play a significant role, and is therefore eliminated in this work. They also observed that the presence or absence of the addition T in the denominator was also not significant. The goodness of fit obtained was the same in either case. In a more recent work, Hauff et al. [9] presented an equation for the oxidation of propene that included the inhibition effects of NO in a different manner. In that case the denominator was:

$$R_I = \left(1 + K_6 Y_{C_3H_6} + K_8 Y_{NO}\right)^2 \tag{23}$$

In Khosravi et al. [13], for an investigation of the reactions of C_3H_6 and NO mixtures, it was observed that the model form proposed by Ref. [9] was equally as good as the Voltz model for both of the catalysts considered here. We have therefore adopted the Hauff version, with the addition of an inhibition term for the CO. Five NO oxidation models were also tested in Ref. [13], with the best result for the two catalysts being given by a model also proposed in Ref. [9]. We therefore arrived at the base model for the three oxidation reactions, which are:

$$(-R_{CO}) = \frac{k_1 Y_{CO} Y_{O_2}}{T^n \left(1 + K_5 Y_{CO} + K_6 Y_{C_3H_6} + K_8 Y_{NO}\right)^2} \tag{24}$$

$$\left(-R_{C_3H_6}\right) = \frac{k_3 Y_{C_3H_6} Y_{O_2}}{T^n \left(1 + K_5 Y_{CO} + K_6 Y_{C_3H_6} + K_8 Y_{NO}\right)^2} \tag{25}$$

Table 4
Parameter values for Models A and B for the platinum catalyst.

Parameter	Model A	Model B
A_1	13.75	12.12
E_1	38,175	34,722
A_2	25.28	24.45
E_2	78,440.	110,793
A_3	11.78	14.30
E_3	48,009	0
A_4	13.83	10.08
E_4	60,619	13,069
B_5	6.901	6.324
H_5	−51,722	−43,005
B_6	7.447	0.5212
H_6	−61.757	−17,239
B_8	8.121	6.814
H_8	−1855. 7	−459.08
B_9	19.98	19.87
H_9	134,718	142,725
B_{10}	13.97	11.87
H_{10}	−72,511	−143,755
A_{11}	26.42	25.65
E_{11}	83,691	107,785
B_{12}	8.258	7.747
H_{12}	−68,027	−82,929
B_{13}	7.530	5.401
H_{13}	−49,974	−56,221
B_{14}	N/A	6.672
H_{14}	N/A	−140,524
B_{15}	N/A	9.566
H_{15}	N/A	−15,373
B_{16}	N/A	9.380
H_{16}	N/A	−51,639

$$(-R_{NO}) = \frac{k_4 Y_{NO} Y_{O_2}^{0.5}}{T^n \left(1 + K_8 Y_{NO} + K_{10} Y_{NO_2}\right)^2} \left(1 - \beta\right) \quad (26)$$

In this base model we have retained the option of including T in the denominator introduced by Ref. [3]. Thus, when $n = 0$ the temperature in the denominator disappears, and when $n = 1$ it is present. Although it was found in Refs. [6,13] that this term had no significant effect on the model fit, it has been retained for the moment, and its impact will be addressed in more detail shortly.

The reduction reactions adopted were based on the best results presented in Ref. [13]. The equations for the production of N_2 and N_2O, respectively are:

$$(-R_{NO})_{r1} = \left(-R_{C_3H_6}\right) \frac{k_2 Y_{NO}}{\left(1 + K_9 Y_{O_2}\right)\left(1 + K_{12} Y_{NO}\right)\left(1 + K_{13} Y_{C_3H_6}\right)} \quad (27)$$

$$(-R_{NO})_{r2} = \left(-R_{C_3H_6}\right) \frac{k_{11} Y_{NO}}{\left(1 + K_9 Y_{O_2}\right)\left(1 + K_{12} Y_{NO}\right)\left(1 + K_{13} Y_{C_3H_6}\right)} \quad (28)$$

We also allow for the reduction of NO_2 (if formed) back to NO by hydrocarbon. Because this reaction is fast, the rate was set to be 10 times faster than the rate of NO reduction, that is:

$$\left(-R_{NO_2}\right) = \left(-R_{C_3H_6}\right) \frac{10 k_2 Y_{NO_2}}{\left(1 + K_9 Y_{O_2}\right)\left(1 + K_{12} Y_{NO}\right)\left(1 + K_{13} Y_{C_3H_6}\right)} \quad (29)$$

The set of Eqs. (24)–(29) is hereinafter referred to Model A. We first performed the optimization for the Pt mono-metallic catalyst. There were ten experiments available. In this case we optimized

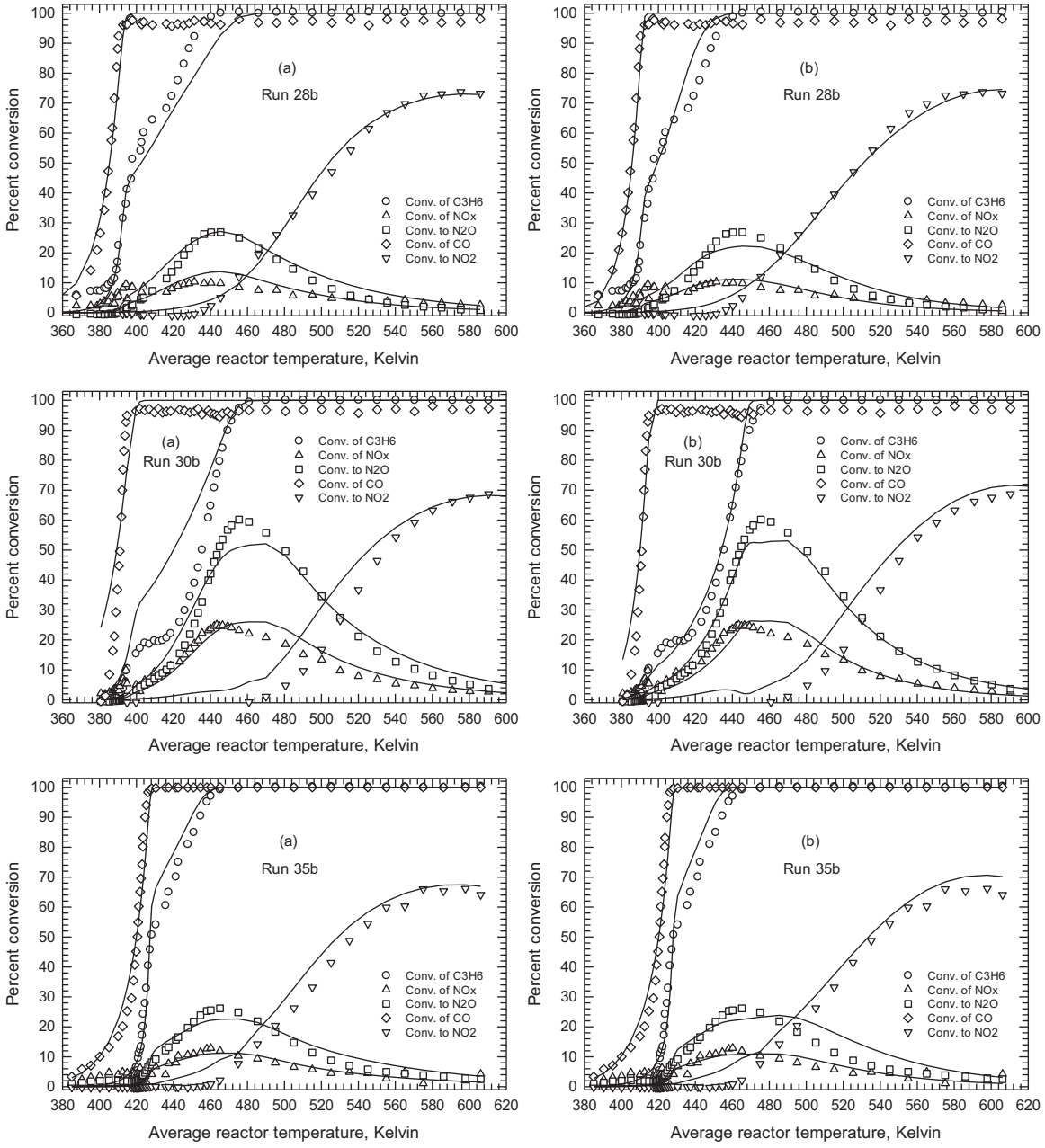

Fig. 8. Comparison of the experimental and model results for three experiments run with the Pt:Pd catalyst. The symbols are the experimental points and the lines are the model predictions. Runs 28b, 29b, 30b, 31b, 32b, 33b, 34b and 35b were used in the curve fitting, which includes the experiments shown here. (a) Model A and (b) Model B.

five experiments (23a, 28a, 29a, 31a and 33a), and then used the resulting parameters to predict the other five experiments (24a, 26a, 27a, 30a and 32a). The five experiments for the curve fitting were chosen from the available data to represent as far as possible the extreme limits of the concentrations used, with the other five therefore being interpolations. It was felt that this was the best test for the model, because it is important to know the usefulness of the model in the prediction of new concentrations not used in the curve fitting. The results are shown and discussed shortly, including the effect of the T in the denominator.

We also investigated the effect of using different parameters in the inhibition terms for the oxidation reactions, rather than common terms. It was observed that some improvement in the model could be obtained if the propene oxidation expression was changed to:

$$\left(-R_{C_3H_6}\right) = \frac{k_3 Y_{C_3H_6} Y_{O_2}}{T^n \left(1 + K_{14} Y_{CO} + K_{15} Y_{C_3H_6} + K_{16} Y_{NO}\right)^2} \tag{30}$$

This model is called Model B. Obviously, this equation introduces six new parameters to the model, resulting in a more time consuming exercise for the parameter determination.

As noted earlier, we retained the option of including T in the denominator. Extensive testing was done with and without the T present, and ultimately it can be concluded that the overall same level of fit can be obtained in either case. Although this observation

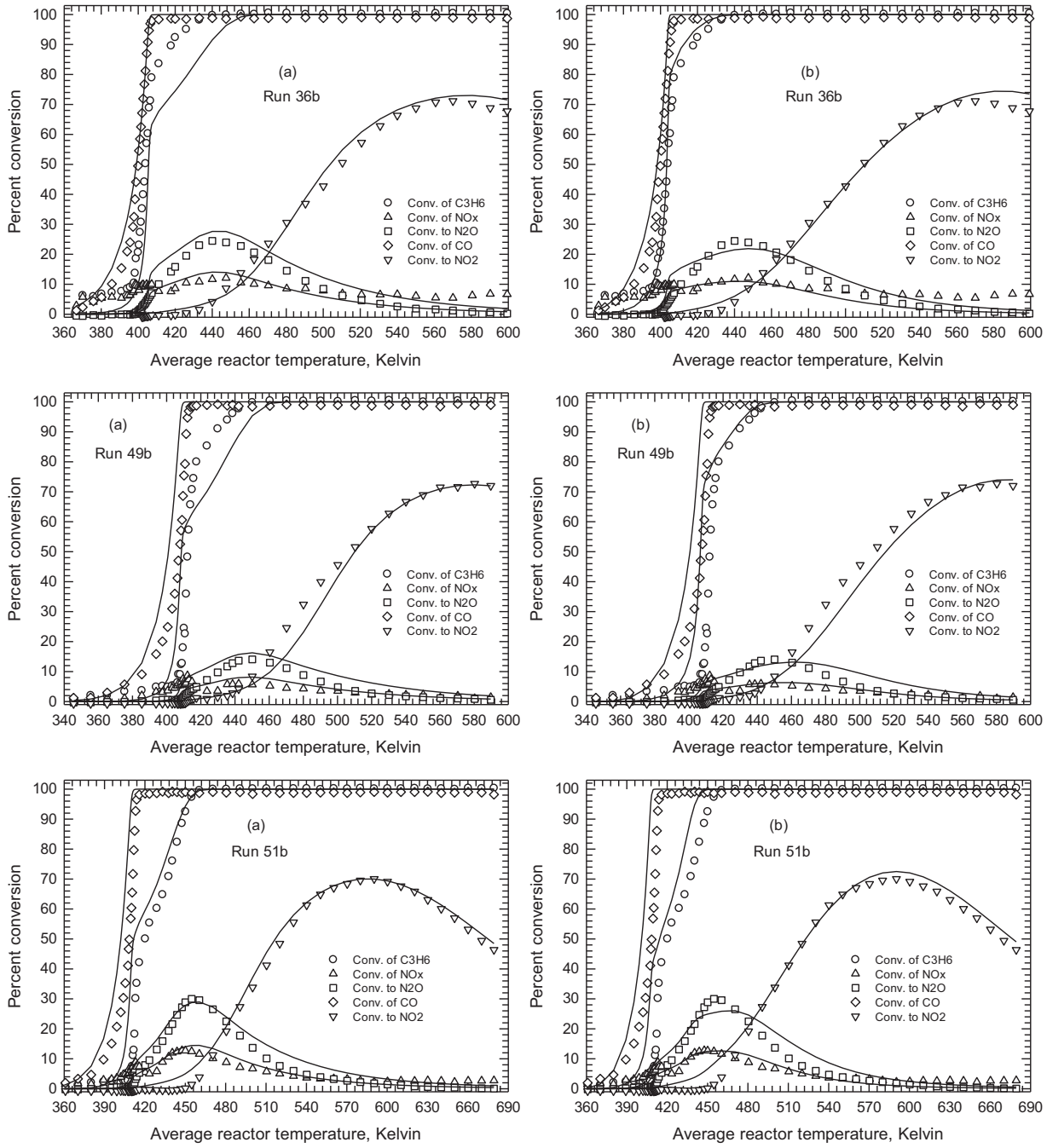

Fig. 9. Comparison of the experimental and model results for three experiments run with the Pt:Pd catalyst. The symbols are the experimental points and the lines are the model predictions. The predictions were made using the parameters determined from the optimization of experiments runs 28b, 29b, 30b, 31b, 32b, 33b, 34b and 35b. (a) Model A and (b) Model B.

may appear to be evident, we feel that some additional explanation may prove useful to modellers in the area.

Consider, for illustration purposes, the oxidation reactions for the Pt catalyst. The rate constants (the terms in the numerator) can be expressed in the form that includes the T from the denominator in the general form:

$$k_i = \exp\left\{A_i - \ln(T) - \frac{E}{R}\left[\frac{1}{T} - \frac{1}{450}\right]\right\} \quad (31)$$

If the temperature is absent, then the rate constant would be written:

$$k_i' = \exp\left\{A_i' - \frac{E'}{R}\left[\frac{1}{T} - \frac{1}{450}\right]\right\} \quad (32)$$

Assume, for the sake of argument, that we have determined the best set of parameters for the model with the temperature present. Then, we pose the question, holding all of the other parameters constant, is it possible to find a value of A' and E' such that $k_i \approx k_i'$ over the temperature range that is important for the reaction in question. It was observed, for example, that if the optimal set of parameters for a set of experiments was determined including the denominator temperature, thus giving a rate constant defined by Eq. (31), it was straightforward to find the equivalent rate constant, given by Eq. (32). The procedure is as follows. Let us define a residual as:

$$R^2 = \left[\left\{A_i - \ln(T) - \frac{E}{R}\left[\frac{1}{T} - \frac{1}{450}\right]\right\} - \left\{A_i' - \frac{E'}{R}\left[\frac{1}{T} - \frac{1}{450}\right]\right\}\right]^2 \quad (33)$$

For the temperature range that is relevant, we then search for values of A' and E' that minimize the residual. When this operation is performed, it was observed that the average difference between k_i and k_i' was of the order of less than 0.05%, which led to no observable difference in the ignition curves. With this observation, it should be concluded that the temperature in the denominator of the Voltz type expressions can be safely dispensed with, which is also consistent with our earlier work [6,13].

All results presented herein after are in the absence of T (that is, $n = 0$). The comparisons for a subset of the 10 experiments are given in Figs. 6 and 7 for Models A and B. Three typical results are selected for each figure. Note that the experiments shown in Fig. 6 were used in the optimization process, whilst those illustrated in Fig. 7 were not. The residuals are given in Table 3, whilst the parameter values are given in Table 4. We observe from these comparisons that the fit is good for the Pt catalyst. The predictive ability of the model is also encouraging. Model B gives better results generally, although the improvement might not be considered significant enough to justify the extra work.

3.4. Kinetic model for the platinum–palladium catalyst

We do not expect the model for the platinum catalyst to be able to predict the apparent two stage propene ignition curve observed for the Pt:Pd catalyst. We do not show the results here, but that was indeed found to be the case. If modelling the two stage ignition is not important, then the model is able to predict an "average" ignition curve, but this approach is not ideal. To improve the model, we start from the observation that the first stage of the ignition curve appears to be related to the presence of CO, and its rate of oxidation. We have already observed that the intersection of the two stages appears when the CO conversion reaches 100%. Therefore

Table 5
Residuals for Models A and B for the Pt:Pd catalyst experiments.

Exp.	Model	CO	HC	NO_X	N_2O	NO_2	Total
28	A	24.3	24.7	10.4	6.0	3.3	68.7
28	B	13.7	24.9	6.9	7.4	4.1	56.9
29	A	13.3	33.7	34.0	38.3	10.3	129.6
29	B	7.4	27.0	31.2	10.9	5.5	81.9
30	A	96.1	144.8	9.3	13.1	19.5	282.7
30	B	46.3	7.8	8.9	5.7	16.9	85.6
31	A	11.2	69.0	50.1	29.8	8.7	168.8
31	B	28.3	34.4	40.8	4.4	6.9	114.8
32	A	62.9	89.9	1.7	0.8	14.5	170.0
32	B	48.9	30.1	1.6	2.2	12.5	95.3
33	A	132.5	95.2	4.9	3.4	12.7	248.7
33	B	51.4	33.5	4.8	2.1	10.5	102.4
34	A	67.8	39.4	2.9	5.1	6.8	122.0
34	B	29.1	4.5	4.1	10.4	7.2	55.3
35	A	27.8	27.0	6.3	4.0	10.1	75.2
35	B	35.1	23.5	5.9	6.7	9.9	81.2
36	A	18.3	113.4	27.7	9.0	4.6	173.1
36	B	46.2	27.9	21.4	10.5	4.3	110.3
37	A	207.6	143.9	7.3	1.7	12.7	373.2
37	B	193.3	190.0	7.2	2.7	10.1	403.3
38	A	95.7	122.4	18.4	14.8	18.1	269.3
38	B	262.4	61.8	10.7	27.6	15.0	377.5
39	A	91.3	123.0	2.7	3.1	8.1	228.2
39	B	168.7	66.6	2.7	6.6	8.9	253.4
40	A	27.2	30.3	14.2	6.7	10.5	89.0
40	B	33.3	14.1	12.8	5.0	11.8	76.9
41	A	19.1	16.7	45.3	17.5	12.6	111.2
41	B	21.4	29.2	36.9	25.5	9.7	122.8
42	A	61.6	13.4	2.2	2.0	3.7	83.0
42	B	61.1	9.7	2.3	5.5	4.8	83.3
43	A	174.2	110.8	5.0	4.3	2.5	296.9
43	B	121.0	70.6	4.3	5.9	2.2	204.0
44	A	25.7	36.5	3.5	3.1	12.6	81.4
44	B	14.1	20.3	2.0	3.4	15.3	55.1
45	A	102.1	37.4	14.3	16.0	11.0	180.7
45	B	52.0	32.7	12.8	5.3	10.2	113.1
46	A	53.4	103.4	5.2	6.0	10.4	178.4
46	B	35.4	17.6	5.2	5.2	9.0	72.4
47	A	108.1	60.1	17.0	8.5	8.0	201.6
47	B	157.1	77.2	13.5	15.6	6.8	270.2
48	A	263.8	95.4	14.3	14.8	6.8	395.0
48	B	471.6	141.4	6.2	32.3	8.8	660.5
49	A	291.7	239.2	5.5	11.6	7.1	555.1
49	B	340.4	582.3	4.3	9.2	8.0	944.1
50	A	19.7	60.2	5.8	5.3	3.6	94.6
50	B	16.2	38.6	4.4	6.2	6.6	71.9
51	A	223.6	198.1	5.9	9.7	4.4	441.8
51	B	323.0	230.1	4.1	13.3	7.1	577.5
52	A	438.2	523.4	13.5	43.3	10.5	1028.9
52	B	430.9	638.7	10.6	38.8	15.1	1134.1
53	A	133.8	106.0	9.7	9.2	6.9	265.5
53	B	303.7	44.8	7.0	14.7	8.7	378.9
54	A	244.1	133.9	2.9	2.8	7.8	391.6
54	B	292.2	144.0	2.8	7.2	8.9	455.1

we propose a modified two stage reaction rate for the oxidation of propene, that is, the modified version of Model A becomes:

$$\left(-R_{C_3H_6}\right) = \frac{k_3 Y_{C_3H_6} Y_{O_2} + k_{17} Y_{C_3H_6} Y_{O_2} (-R_{CO})}{T^n \left(1 + K_5 Y_{CO} + K_6 Y_{C_3H_6} + K_8 Y_{NO}\right)^2} \quad (34)$$

where in this work $n = 0$. When fitting these experiments, we selected a representative range of eight runs, optimized the parameters, and then tested to see if the resulting model could predict the remaining experiments. The eight runs selected were 28b, 29b, 30b, 31b, 32b, 33b, 34b and 35b. These eight runs represent a full factorial analysis of the three species for a low and a high concentration. The remaining runs represent experiments that contain at least one species at the intermediate concentration. The results for a subset of the experiments are shown in Figs. 8 and 9 for both Models A and B. Fig. 8 shows three typical results from the subset used to

Table 6
Parameter values for Models A and B for the Pt:Pd catalyst.

Parameter	Model A	Model B
A_1	15.86	15.48
E_1	52,091	16,914
A_2	16.59	26.43
E_2	0	72,255
A_3	10.45	12.52
E_3	146,620	120,744
A_4	8.717	8.028
E_4	13,450	24,836
B_5	8.303	8.232
H_5	−27,065	−41,748
B_6	6.701	2.382
H_6	−25,308	−149,999
B_8	7.161	7.344
H_8	−20,228	−33,665
B_9	11.15	21.32
H_9	60,688	139,642
B_{10}	12.25	11.12
H_{10}	−149,524	−150,000
A_{11}	17.28	27.14
E_{11}	2012.5	77,293
B_{12}	9.393	9.577
H_{12}	−35,901	−87,411
B_{13}	7.173	0.00
H_{13}	−95,115	−0.26
B_{14}	N/A	9.593
H_{14}	N/A	−15.58
B_{15}	N/A	8.914
H_{15}	N/A	−31,417
B_{16}	N/A	8.356
H_{16}	N/A	−5849.2
A_{17}	11.81	14.05
E_{17}	0	9401

determine the parameters, whilst Fig. 9 shows three typical results for the experiments not used in the optimization, using the same parameters. The residuals are given in Table 5, whilst the parameter values are given in Table 6. The model appears satisfactory, although the sharpness of the transition in the propene oxidation curve is not always reproduced well.

Overall the LHHW type models proposed appear to give an adequate representation of the ignition curves, and their predictive ability is also encouraging. Obviously the parameter values found here would not be applicable to other catalysts, however, the form of the model should have a good chance of success. A constant theme through the sequence of three papers (Refs. [6,13], and this work) is that the stepwise determination of model parameters is not effective. That is, one cannot independently determine the parameters from single reactant experiments. The same point is made here. That is, we could not use the parameters generated for the C_3H_6 and NO mixtures (generated in the work of Ref. [13]) in the model obtained when CO was added. Therefore, kinetic parameters should be determined from experiments containing all reactants.

4. Conclusion

This work has investigated the reactions of CO, C_3H_6 and NO in a lean synthetic automobile exhaust gas over Pt and Pt–Pd diesel oxidation catalysts. An abnormal behaviour for propene ignition curve was observed in the case of the Pt:Pd catalyst. Models for the oxidation reduction reactions were formulated of the LHHW type. For the Pt:Pd catalyst a two-step oxidation model was used for the C_3H_6 oxidation curve. The models proposed fit the data reasonably well, and have some predictive ability when applied to experiments not used in the curve fitting.

Appendix A. Supplementary data

Supplementary data associated with this article can be found, in the online version, at http://dx.doi.org/10.1016/j.apcatb.2014.02.001.

References

[1] R.M. Heck, R.J. Farrauto, S.T. Gulati, Catalytic Air Pollution Control, Commercial Technology, Wiley, New York, 2009.
[2] S. Voltz, C. Morgan, D. Liederman, S. Jacob, Industrial & Engineering Chemistry Product Research and Development 12 (1973) 294–301.
[3] S.H. Oh, J.C. Cavendish, L.L. Hegedus, AIChE Journal 26 (1980) 935–943.
[4] S.H. Oh, J.C. Cavendish, Industrial & Engineering Chemistry Product Research and Development 21 (1982) 29–37.
[5] S.H. Oh, J.C. Cavendish, AIChE Journal 31 (1985) 935–942.
[6] C. Sola, A. Abedi, R.E. Hayes, W.S. Epling, M. Votsmeier, Canadian Journal of Chemical Engineering (2014), http://dx.doi.org/10.1002/cjce.21961.
[7] G.C. Koltsakis, I.P. Kandylas, A.M. Stamatelos, Three-way catalytic converter modeling and applications, Chemical Engineering Communications 164 (1998) 153–189.
[8] A. Pandya, J. Mmbaga, R.E. Hayes, W. Hauptmann, M. Votsmeier, Topics in Catalysis 52 (2009) 1929–1933.
[9] K. Hauff, U. Tuttlies, G. Eigenberger, U. Nieken, Applied Catalysis B: Environmental 100 (2010) 10–18.
[10] C. Sola-Quiroz, M. Sc, Department of Chemical and Materials Engineering, University of Alberta, Edmonton, AB, Canada, 2011.
[11] M. Khosravi-Hafshejani, M. Sc, Department of Chemical and Materials Engineering, University of Alberta, Edmonton, AB, Canada, 2013.
[12] C. Sampara, E. Bissett, M. Chmielewski, D. Assanis, Industrial & Engineering Chemistry Research 46 (2007) 7993–8003.
[13] M. Khosravi, C. Sola, A. Abedi, R.E. Hayes, W.S. Epling, M. Votsmeier, Applied Catalysis B: Environmental 147 (2014) 264–274.
[14] S. Salomons, R.E. Hayes, M. Votsmeier, Applied Catalysis A: General 352 (2009) 27–34.